Sulphur Variations in Annually Layered Stalagmites Using Benchtop Micro-XRF

Huixin Wang,[a] Pauline Treble,[b, c] Andy Baker,[b, c, e] Anne M. Rich,[a] Saroj Bhattacharyya,[a] Fabio Oriani,[d] Rabeya Akter,[a] Khorshed Chinu,[a] Irene Wainwright,[a] Christopher E. Marjo*[a,e]

[a] Mark Wainwright Analytical Centre, Chemical Sciences Building (F10), University of New South Wales, Kensington, NSW, Australia 2052

[b] School of Biological Earth and Environmental Sciences, University of New South Wales

[c] Australian Nuclear Science and Technology Organisation, Lucas Heights, NSW Australia 2234

[d] Institute of Earth Surface Dynamics, Université de Lausanne, Switzerland

[e] Earth and Sustainability Science Research Centre (ESSRC), School of Biological, Earth and Environmental Sciences, University of New South Wales, Sydney, NSW, 2052, Australia

*Corresponding author. Tel.: +612 9385 4693; fax: +612 9385 4663.

E-mail address: c.marjo@unsw.edu.au

Abstract

Variation of sulphur in annually laminated stalagmites can be used to infer the impact of past volcanic activities, anthropogenic pollution, and climate change due to increased bushfire activity. The synchrotron radiation micro-X-Ray fluorescence (SR-XRF) microprobe is a powerful tool to analyse and image sulphur recorded in stalagmites with micrometre resolution. However, access to SR-XRF beamlines can be limited, so researchers must select the most promising stalagmites for imaging. Benchtop micro-XRF is an effective tool for trace elemental analysis of speleothem samples and is a candidate for routine laboratory measurement of sulphur along stalagmite laminae and screening for SR-XRF. This study describes a protocol using matrix-matched standards to measure annual variations of sulphur at trace to percent level along the laminae of two Western Australian stalagmites, one of which already having been analysed using SR-XRF. Parameters that affected quantitation include X-ray tube voltage and current, spot size of the X-ray beam and stalagmite surface roughness and porosity. The use of a 20 μm X-ray spot size provides sub-annual spatial resolution that can be completed in an overnight scan. The features in a 1000 point micro-XRF analysis of sulphur along a 20 mm transect show good consistency with SR-XRF microprobe data. Micro-XRF mapping was also performed to produce chemical images on the stalagmite and compared with Raman and X-ray diffraction (XRD) to confirm that the stalagmite is exclusively calcite, with no aragonite, and that the source of sulphur in the samples was gypsum and anhydrite. Regions of very high sulphur in the micro-XRF maps were found to be artefacts due to diffraction of the incident beam but these could be efficiently removed by using a multiple point statistics approach to produce a clean image suitable for analysis of the laminae. This work shows the potential of micro-XRF for routine analysis of sulphur in stalagmites, and to streamline sample characterisation before SR-XRF imaging.

Keywords: stalagmite, synchrotron, micro-XRF, sulphur, Raman, multipoint statistics.

Introduction

Stalagmites are a type of speleothem, a calcium carbonate deposit formed in limestone caves. These deposits form from drip water that is supersaturated with respect to calcite or aragonite due to the dissolution of carbonate bedrock between the surface and the cave. Stalagmites grow vertically upwards from the cave floor, and most are formed from calcite. This calcite contains trace amounts of elements that reflect the drip water chemistry of the site. Typically, the highest concentration elements after Ca are those most abundant in limestone, namely Mg, Sr, Ba and U. Trace amounts of soil-derived elements (for example, P, S and soil minerals Ba, Fe, Zn) may also be present, depending on the hydrological connectivity of the drip water to the soil. It is well known that this suite of trace elements (e.g., Mg, S, P, Sr, Ba, Fe, Zn) incorporated into the calcareous stalagmite provides information on past environmental change [1][2].

Variations of sulphur in speleothems is closely linked to volcanic events, bushfire and industrial activities [3][4][5]. Sulphur concentrations in stalagmite samples have significant advantages as records of these events: stalagmites are widely found in continental areas and they grow in relatively protected environments that are free from re-deposition and alteration. The concentration of sulphur in stalagmite samples can be used to reflect the atmospheric sulphur loading [3]. The chronologies of stalagmite can be obtained by absolute radiometric methods [5], however, the transmission of sulphur from atmosphere to soil, and eventually to stalagmite in the drip sites, can be significantly lagged by up to a few decades and attenuated due to secondary processes, such as uptake by vegetation [6][7], biogenic activity and soil storage [8][9].

The amount of sulphur incorporated into stalagmite samples is commonly at ppm levels requiring techniques with high sensitivity capable of detecting a wide range of elements. Techniques, such as secondary ion mass spectrometry (SIMS) [10], laser ablation inductively coupled plasma mass spectrometry (LA-ICP-MS) [11][12][13], and optical emission using laser induced breakdown spectroscopy (LIBS) [14][15][16] are used on stalagmites that ablate material directly from the stalagmite surface. For SIMS, spot sizes well below 10 μm offer sub-annual spatial resolution to allow the study of seasonal variations of trace elements within a single lamina. However, ablation techniques are mildly destructive, leaving a narrow track along the sample, which may not meet some research needs. Also, the ablation or ionisation is very sensitive to a rough or porous surface, or the variation in mineral matrix requiring careful selection of matrix matched standards for calibration [10][13]. Solution-based ICP-MS analysis of stalagmites is also possible, where drilled powders from each laminae are dissolved in dilute acid. This method can detect elements at the ppb-ppm level, however, the drilling and digestion process is time consuming and challenging for small lamina,

requiring much attention to achieve reliable results [2][17][18]. The experience of sulphur measurement by the authors using a standard, single quadrupole ICP-MS instrument, whether by solution nebulisation or laser ablation, is mass interference, for example, attempting to measure ^{32}S is problematic due to the abundant $^{16}O_2$ molecular ion. An alternate approach commonly used to avoid mass interference is measuring the oxide, $^{32}S^{16}O$, but this has an interference from the ^{48}Ca isotope, which has a natural abundance of only 0.187% but this becomes a significant problem for measuring trace sulphur in a calcium carbonate matrix.

Recent years have seen synchrotron radiation micro-X-Ray fluorescence (SR-XRF) microprobe as a powerful, non-destructive technique to determine the variations of trace elements in speleothems to reconstruct past climate change [19][20][21]. This technique has also been applied for interpreting sulphur concentrations in stalagmites to study past volcanic eruptions following the pioneering work of Frisia and co-workers [21]. SR-XRF is of great advantage for sulphur analysis due to its extremely low background, high spatial resolution (~2 μm) and low detection limit to sub-ppm level [3][17]. In addition, by coupling SR-XRF with X-ray near absorption near-edge structure spectroscopy (XANES), not only concentration but also oxidation state information can be obtained simultaneously, thus the origin of sulphur can be traced [22]. However, SR-XRF beamlines tend to be heavily oversubscribed so researchers must select the most promising stalagmites for imaging. Other X-ray fluorescence techniques include geological core scanners, but these usually lack the spatial resolution requirements for analysis within a single growth layer. Techniques such as the nuclear microprobe or the scanning electron microscope with energy dispersive X-ray analysis (SEM-EDX) can be limited by the small size of the sample chamber, or the detection limits are inadequate for measuring variation in sulphur at ppm levels [23][24]. There remains a demand for additional cost-effective, laboratory-based tools for elemental variation analysis of stalagmite samples.

Laboratory benchtop micro-XRF has been introduced as a fast, non-destructive elemental analysis tool with spatial resolution of tens of micrometres, benefiting from recent developments in X-ray optics that make the best use of low power, sealed-tube X-ray sources [25]. Although the technique is yet to achieve the sensitivity and spatial resolution of SR-XRF, laboratory-based micro-XRF is relatively inexpensive and has major advantages such as rapid local access to elemental concentration and mapping analysis, minimal sample preparation, the capability to analyse a wide range of sample types and size. This technique has been applied for trace element analyses of speleothems and other calcium carbonate samples [26][27]. However, the potential of this technique in the application of sulphur variation analysis of speleothem samples has not been fully developed to date. Dandur and and co-workers collected the first sulphur mapping data of a stalagmite sample using micro-XRF and showed that sulphur distribution is consistent with laminae of the concretion [28]. Recently, Vansteenberge *et al.* systematically investigated the potential of benchtop micro-XRF for the analysis

of trace element in stalactites and stalagmites [29]. A range of measuring conditions were tested, and the results evaluated by comparison with ICP-MS data on the same sample. Reliable results were obtained for calibrations of Mg, Al, Si, P, Ca, Mn, Fe, Zn, Sr and Ba but correlation for sulphur was poor with a Pearson's *r* value of 0.07. The quantification result obtained by micro-XRF was determined not only by chemical composition but also variation in matrix crystallinity along a stalagmite. Changes in crystal fabric, mineral polymorphs such as calcite and aragonite and varying degrees of porosity are commonly found in stalagmite samples [30] and this will be reflected in the XRF spectra and thus affect the quantification result.

In this work, the variation of sulphur along annual laminae in two stalagmites was measured using a commercial rhodium-source benchtop micro-XRF. The measuring conditions assessed were X-ray tube voltage, current and sample surface smoothness. Seven matrix-matched pressed pellet standards, from 50-2000 ppm, were prepared for calibration and quantification analysis. A 1000 point micro-XRF analysis of sulphur along a 20 mm transect of an annually layered stalagmite from Yonderup Cave in Western Australia was carried out to analyse the variations of sulphur over the period AD 1725-2000 and compared favourably with SR-XRF data from the same sample. The potential of micro-XRF to capture the seasonality of sulphur to derive high-resolution chronologies was investigated using a second sample from Quininup Cave in Western Australia. Micro-XRF mapping analysis of this sample was supplemented with Raman mapping and XRD to show that the sulphur banding was due to a mixture of gypsum and anhydrite in the sample. Artefacts appearing as high sulphur regions were identified as diffraction of the incident X-ray beam. These artefacts could be successfully removed using multiple point statistics to reveal the laminae.

Experimental/Methods and Materials

Stalagmite samples

An annually layered stalagmite, YD-S2, was harvested from Yonderup Cave (31°33′S, 115°41′E) located in Yanchep National Park, Western Australia, about 47 km north-northwest of Perth. Yonderup Cave is formed in Tamala Limestone, a Late Quaternary age aeolianite that is widely found along the coast of south-west Western Australia. The aeolianite comprises mostly carbonate and quartz, with < 3% microcline and orthoclase feldspar [31]. The trace element record of YD-S2 was derived from previously published LA-ICP-MS line profiles that demonstrate annual variations in a suite of bedrock-derived (Sr, Ba, U) trace elements [32]. Drip water geochemistry at this site has also been investigated, specifically to investigate the possible impact of wildfire [33]. The stalagmite was deposited over the last 250 years and an existing chronology was available from variation in the LA-ICP-MS Sr concentrations that was optimised using visible laminae counting and SR-XRF of Sr [34].

A second stalagmite, QU_test1, from Quininup Lake Cave is located on the Leeuwin-Naturaliste Ridge near the town of Wilyabrup (33°47′S 115°2′E) and is also developed in the Late Quaternary aeolianite that skirts the southwest coastline of Western Australia. The cave is approximately 300 m from the current coastline with a doline entrance that faces the ocean. The climate is Mediterranean-type with wet winters and dry summers. The nearest climatological station is Cowaramup (station ID 9636) with annual rainfall of 1134 mm. Dry aerosol deposition at the cave site is likely to be significant given the proximity to the coast and prevailing westerly winds. Mean annual temperature along this coastal region is approximately 20 deg C. The local vegetation is low lying coastal scrub dominated by *Acacia.* An archaeologically significant site is to the north of the cave at Quininup Brook [35]. QU_test1 was measured as an unpolished and polished sample, with polishing achieved using successively finer grades of corundum-based sandpapers followed by successive polishes with 9, 3, and 1 µm diamond paste on a mechanical polisher. The polishing residue was removed with AR grade methanol and samples ultrasonicated in MilliQ water prior to measurement.

Benchtop Micro-XRF

All micro-XRF experiments were carried out on a benchtop M4 Tornado micro-XRF (Bruker, Germany) under vacuum condition (20 mbar). The instrument consists of a Rh anode metal-ceramic X-ray tube with maximum power, voltage and current of 30 W, 50 kV and 600 µA, respectively. There are two silicon drift detectors on this system, referred to as "detector one" and "detector two". Detection limit and precision for the sulphur K line were optimised at 10 kV and 400 µA (Supporting data, **Table S1**). X-ray spot calibration was carried out by digital tuning of the X-ray position indicated on the screen to align with the physical position on the sample. In this study, the voltage and current were optimised to achieve the best spectral resolution for trace quantities of sulphur. The instrument has set spot sizes of 20 µm and 160 µm. To achieve the best spatial resolution, a 20 µm spot size was used throughout. The actual lateral spatial resolution depends on the energy of the fluorescing X-rays with spatial resolution improving at higher X-ray energies. For the Bruker M4 Tornado, the manufacturer provides a spatial resolution of 15.2 µm for the Mo K line (17.4-19.6 keV) and 33.4 µm for the Mo L line (2.3-2.5 keV). The S K_α line (2.31 keV) is close to that of the Mo L_α line (2.29 keV) so the spatial resolution for S K_α in these experiments is estimated to be 33.4 µm. Unless stated otherwise, a single silicon drift detector was used to count the fluorescing X-rays with an energy resolution ≤145 eV full width at half maximum, for Mn K_α. Linescans were conducted in the "auto-point analysis" workspace where each point on YD-S2 (Figure 1A) was measured for 60 seconds with the autofocus function activated to ensure a constant distance between each measured point and the detector. The autofocus function calculates a contrast value at the measured point and assumes that the focal plane has the highest contrast value. Compared to the linescans, micro-XRF mapping of QU_test1 required a shorter measurement time of 300 ms per point with a step size of 40 µm (Figure 1B) to complete the mapping within a reasonable timeframe (<24 hours). Data processing

was performed using M4 Tornado built-in software, FP MQuant (Bruker, Germany) for peak identification however, quantification of sulphur was performed independently using matrix matched standards.

Preparation of matrix matched synthetic sulphur standards for method calibration

Matrix matched, synthetic sulphur standards were prepared as pressed pellets for the following approximate concentration range: 0, 50, 100, 200, 500, 1000, and 2000 ppm (mg/kg). Each standard was produced by adding the required aliquot of an ICP reference solution (HPS, USA) containing sulphur (as sulphate) to 2g of powdered, ultrapure $CaCO_3$ (Merck, Germany). MilliQ water was added to produce a slurry before drying at 50 °C overnight. The dried sample was transferred into a tungsten carbide grinder and crushed using an Essa ring mill (Model LM2, Australia) for 10 min to ensure complete homogenisation. Pellet preparation was performed using 50 mg of the powdered $CaCO_3$ on a Mini-Pellet Press (Specac, UK) to produce a pellet 7 mm diameter and 1mm thick. Subsamples (200mg) were digested using 20% HNO_3 in a hot water bath and analysed using inductively coupled plasma-optical emission spectrometer (ICP-OES, PerkinElmer, USA) to confirm the sulphur content in each standard as 0, 55, 71, 146, 624, 1134 and 2089 ppm (supporting data **Table S2**).

Synchrotron micro-XRF Imaging

Synchrotron XRF mapping of YD-S2 has been reported previously [34]. Briefly, relative sulphur concentrations were mapped on beamline 10.3.2 at the Advanced Light Source (ALS) synchrotron located at Lawrence Berkeley National Laboratory in California, USA. The incident energy was 3.988 keV (50eV below the Ca K-edge), and the XRF map was produced using a 7x7 µm incident beam with 200 millisecond dwell time recorded with an Amptek FAST XR-100SDD single element detector. A line plot of the XRF map was extracted using ImageJ software to produce relative concentrations at 10 µm intervals. Absolute concentrations are not available, so the data is presented as relative sulphur concentration for comparison with the benchtop micro-XRF data.

Raman Spectroscopy

Raman spectroscopy and mapping were performed on an inVia Raman microscope (Renishaw, UK) using a long wavelength 830 nm diode laser selected to minimise fluorescence interference that was observed using the more common 532 nm excitation source. Fast mapping data was collected over 23,000 × 1000 µm region using line focus optics in the instrument's "Streamline" mode with a static scan centred at 680 cm^{-1} and acquired over a spectral range of 113-1187 cm^{-1}, using a 10 s exposure, a 20x objective and a 1200 l/mm grating. The estimated power at the sample under these conditions was 165 mW. Data was processed using the WiRE software (Version 5.3, Renishaw, UK) to correct the baseline and remove cosmic rays, then generate an intensity map of the peak centred at 1018 cm^{-1} corresponding to the sulphate stretching band for anhydrite ($CaSO_4$)

X-Ray diffraction

X-Ray diffraction data was collected on an Empyrean diffractometer (PANalytical, Netherlands) fitted with a Co tube. The polished stalagmite sample was mounted on a flat sample stage with careful height adjustment and BBHD optics fitted to the incident beam and a PIXCel detector in the diffracted beam. Data collection was performed over the angular range 5° to 120° with a step size of 0.013°. The raw data was processed using HighScore Plus software (PANalytical, Netherlands) and a set of candidate crystalline phases identified using the ICDD powder diffraction database (International Centre for Diffraction Data, USA).

Multiple point statistics micro-XRF image

Elemental mapping of speleothems can be compromised by irregularities in the calcite surface caused by fabric porosity and damage to the surface during cutting and polishing, effectively producing data gaps or artefacts in the resulting image. These features are readily visible in the calcium maps denoted by Ca concentrations that are lower than 40.04%. Image analysis was performed using a custom filter to detect data gaps using the calcium maps and then the MPS distribution Quick Sampling [36] was used to fill in missing data in the elemental maps with stochastically generated values. The MPS technique mimics data patterns present in the rest of the image with the goal to preserve continuous laminae features. A cross-validation was performed using fake gaps to assure all relevant statistical properties were preserved in the simulated heterogeneity of the image. The aim of this supervised analysis was to find a balance among geometrical properties and statistical properties to achieve an acceptable image.

Results and Discussion

White light images of stalagmites YD-S2 and QU_test1 are shown in **Figure 1**. There is clear contrast in laminations along the growth axis of these samples, which decreases in age from left to right. Previous measurements have confirmed that the variation in Sr concentrations in YD-S2 can be correlated to annual growth [32,34], which is important for our interpretation of sulphur variations in the XRF measurements. The micro-XRF linescan on YD-S2 and the mapped region on QU_test1 are highlighted in red in the figure. Prior to micro-XRF mapping, single-point analysis was performed on YD-S2 to evaluate the effect of the X-ray tube parameters on the signal from sulphur in the sample.

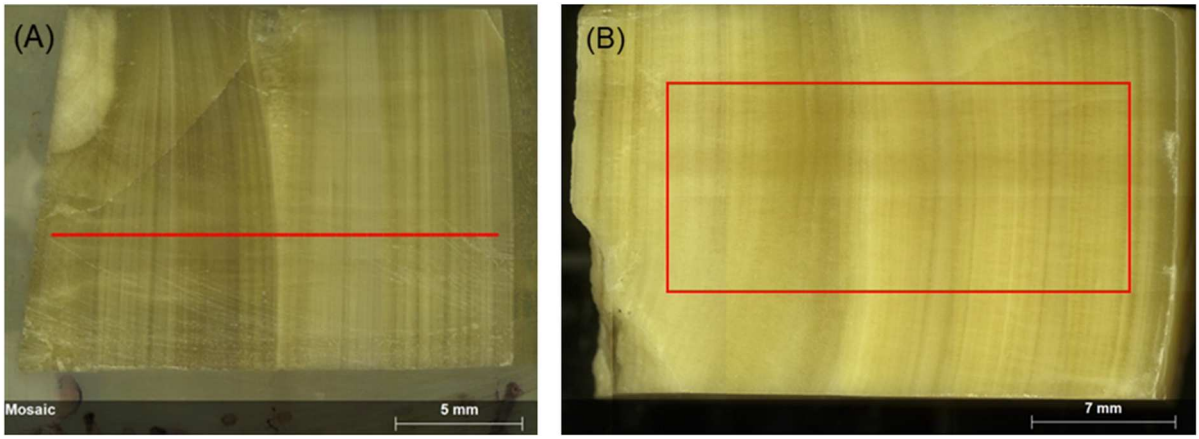

Figure 1. White light images of stalagmites (A) YD-S2 with red line indicating the position of the micro-XRF linescan and (B) QU_test1 with the red box indicating the position of the micro-XRF map.

Optimisation of X-ray tube voltage and current conditions

A Micro-XRF spectrum from a single point analysis of stalagmite YD-S2 is shown in **Figure 2** using a log scale for count rates to observe the trace element peaks. As expected, the K lines from Ca are the strongest peaks followed by K lines from Sr then K lines of trace elements including Mg, Al, and S. In addition to the fluorescence peaks of the major and trace elements in the stalagmite, X-ray tube peaks, including second order Rh K lines (Compton and Rayleigh peaks), are observed at their characteristic energies (18.9-22.7 keV). Certain peaks are observed that do not correspond to emission lines from any element, escape peak or detector sum peaks. These are likely to be diffraction peaks scattered from the crystalline calcite matrix [1].

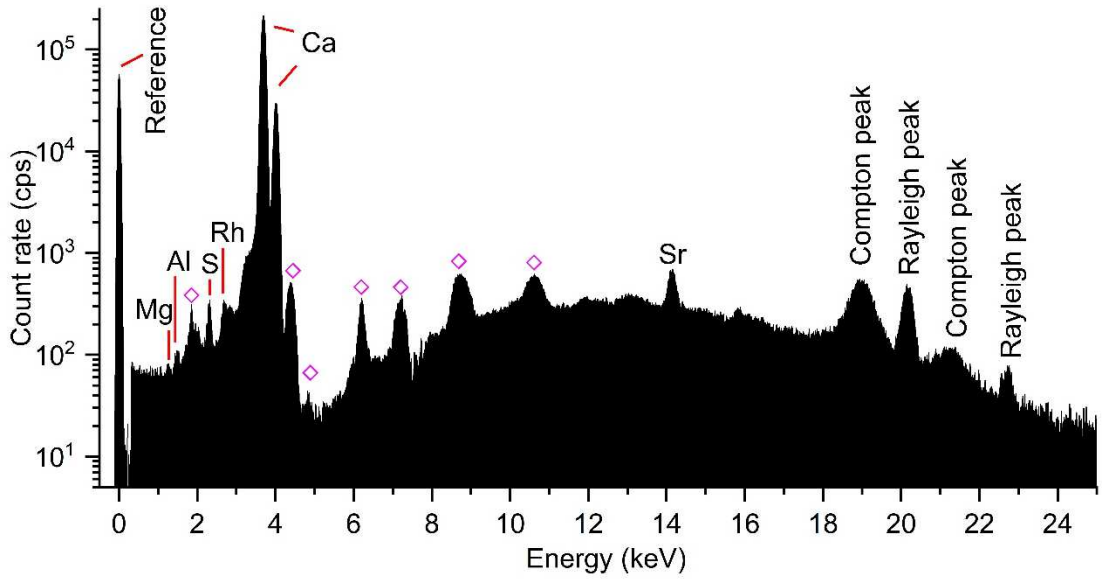

Figure 2. (A) single point micro-XRF spectrum of YD-S2 from 0 to 25 keV, collected at 10 kV, 400 μA for 60 s. The Compton and Raleigh scattering peaks are labelled, and peaks arising from diffraction by the calcite matrix are denoted by magenta diamonds.

Compared to the major elements Ca and Sr, the peak intensity of sulphur is very low with a signal/noise ≤ 2.5, thus accurate quantification of these peaks requires optimisation of the tube voltage and current. This was achieved by measuring a single point of the blank and the 500 ppm sulphur standard and compare to the micro-XRF spectrum of sulphur as the voltage was tuned from 5 to 45 kV and current tuned from 185 to 400 μA. The blank spectrum give a peak centred at 2.35 keV which doesn't correspond to any element X-ray lines or escape peaks. It is likely a diffraction peak caused by crystallinity of the matrix (**Figure 3A**). This peak partially overlaps the sulphur K_α line (2.31 keV) thus can interfere sulphur detection. The intensity of the interference peak dropped significantly when the tube voltage is decreased to 10 keV. Similarly, micro-XRF spectra of the 500 ppm sulphur standard also shows a significant decrease in peak intensity at 2.3-2.35 keV when the tube voltage was decreased to 10 kV (**Figure 3B**). Several statistics, including Figure of Merit (FOM), lower limit of detection (LLD) and relative standard deviation (RSD), were calculated to determine the optimal combination of tube voltage and current using the 500 ppm standard. The optimum counting statistics, lowest detection limit and acceptable precision for the sulphur K line was reached at 10 kV and 400 μA (Supporting data, **Table S1**) and used for the subsequent micro-XRF linescan measurements of sulphur. As the sulphur K line is excited by low energy tube lines (including Rh L lines and continuum X-rays), a decrease in tube voltage can reduce interferences such as diffraction and calcium escape peaks, while leaving sulphur response relatively unaffected, thus can improve the reliability of the method for sulphur quantification.

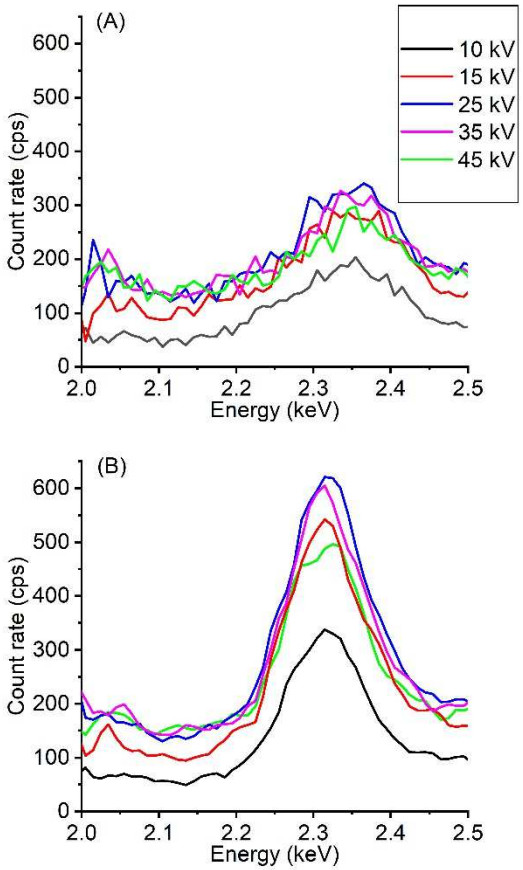

Figure 3. Micro-XRF sulphur spectra of (A) 0 ppm and (B) 624 ppm sulphur standard using tube voltage of 10, 15, 25, 35, 45 kV shown in black, red, blue, pink and green, respectively. A tube current of 400 μA was used.

Calibration for sulphur quantification analysis

To evaluate the feasibility of trace sulphur quantification, a 24-point analysis across 7 synthetic matrix-matched sulphur standards (0, 55, 71, 146, 624, 1134 and 2089 ppm) where the sulphur content was independently determined using ICP-OES (Supporting data, **Table S2**). The X-ray counts of the sulphur K line (after blank subtraction) correlated strongly with the sulphur concentrations from ICP-OES with a Pearson's r value of 0.999 (**Figure 4A**). The limit of detection (LOD) was calculated to be 80 ± 11 ppm (see Supporting data for the calculations). This relationship between the net sum of sulphur K line X-ray counts with concentration was used to calibrate the X-ray counts for sulphur in the stalagmite measurements.

The particle size of the milled powder used to prepare the pressed pellet standards can significantly influence the precision of the data. When the standards were mixed manually, without mechanical grinding, the standard deviation of the net sum values of 624 ppm standard was 295%. When grinding

in a ring mill for 10 minutes, the standard deviation improved to 9% indicating a substantial increase in homogeneity (**Figure 4B**).

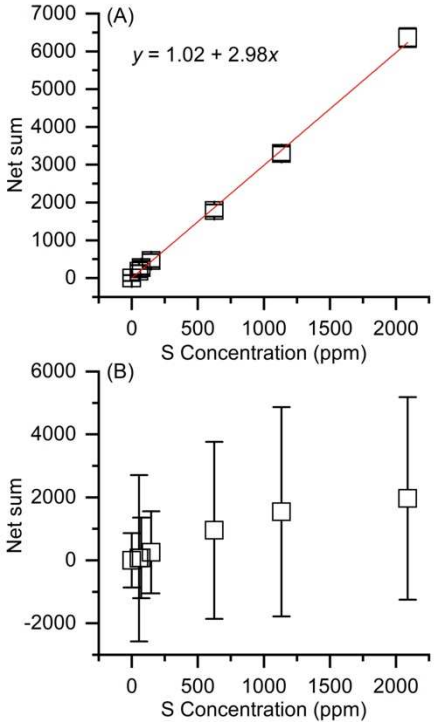

Figure 4. A plot of sulphur net sum counts measured using micro-XRF vs sulphur concentration. Samples were measured (A) with grinding for 10 min and (B) without grinding.

Sulphur quantification analysis of stalagmite samples

Micro-XRF of geological samples ideally requires a polished surface as fluorescing X-rays will undergo different degrees of absorption as they are emitted from a crack on the surface. Also, uncontrolled scattering of the X-rays due to porosity of the sample can cause random changes in the count rates and a high background signal [28][29]. The importance of polishing was tested by comparing a 1000-point linescan of sulphur along a 29.0 mm long transect of QU_test1 before and after polishing. The position of the linescan was noted and estimated to be reproduced within 1-2 mm before and after polishing. The 75 points from the edge measurements at either end of the stalagmite were discarded to produce a dataset of 925 points for the unpolished and polished sample.

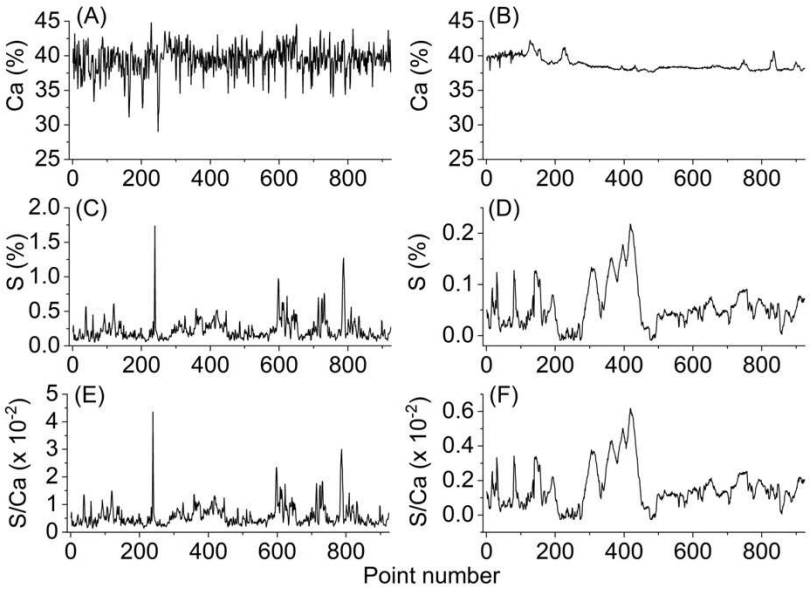

Figure 5. Sulphur micro-XRF linescan of QU_test1 before (left) and after polishing (right). Variation of calcium % (A) before and (B) after polishing. Sulphur % (C) before and (D) after polishing and S/Ca ratio (E) before and (F) after polishing.

The calcium linescan of the unpolished QU_test1 stalagmite shows notably more variation compared to that of the polished one. Fluctuations are present in the unpolished sample that may indicate changes in the roughness that decrease the X-ray fluorescence due different degrees of absorption and scattering by the matrix. Measurements of the unpolished sample have an average calcium concentration of 39.66% ± 2.78% along the 925 points of the linescan (**Figure 5A**) versus 38.78% ± 1.29% after polishing (**Figure 5B**). The concentration of calcium, as calcite, is present at several orders of magnitude higher than the trace elements, so the micro-XRF should show a constant concentration along the linescan and reducing surface features by polishing does improve the standard deviation of the calcium measurement, as observed.

For sulphur, positive spikes up to 1.74% are observed in the linescan of the unpolished sample (**Figure 5C**) while polishing reduces the maximum spike to 0.20% (**Figure 5D**) and the same relative behaviour is shown in the normalised S/Ca ratio (**Figure 5E-F**). The negative spike in the calcium value at Point 239 (**Figure 5A**) corresponds to a high sulphur spike (**Figure 5C, 5E**) but this feature was removed after polishing. Reducing surface roughness through polishing is critical to remove artefacts that indicate unrealistic sulphur values along a stalagmite.

Benchtop micro-XRF vs Synchrotron micro-XRF

To validate the quantification of sulphur on YD-S2, a linescan was measured for comparison with the same region measured by SR-XRF. The measurement comprised a 1000-point analysis along an 18.7 mm transect resulting in an acceptable measurement time of 17 hours. The results show that, although the tube spot size and step size of micro-XRF is twice as large as that of SR-XRF, the major features of the SR-XRF scans can be captured by a benchtop system (**Figure 6A** and **Figure 6B**). A comparison of 25 diagnostic points (either peak or trough values) from the micro-XRF and SR-XRF data shows a strong positive correlation between the two techniques (r = 0.97, **Figure 6C**), which supports the feasibility of using micro-XRF to streamline sample characterisation for SR-XRF imaging.

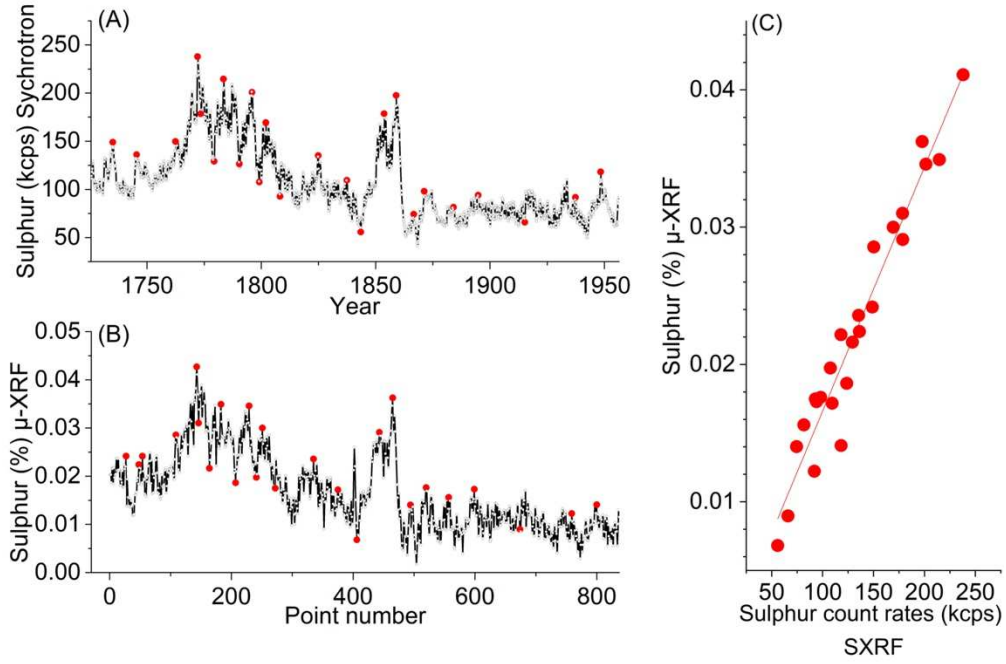

Figure 6. Single point analysis of sulphur on YD-S2 over year 1725-1956 obtained by (A) SR-XRF with a step size 10 µm; (B) M4 Tornado micro-XRF with tube spot size 20 µm, step size 19 µm. (C) Sulphur concentration of selected points obtained by micro-XRF *vs* sulphur count rates of the same positions measured using SR-XRF. Solid red circles denote the selected points used to plot the correlation between the sulphur values measured by micro-XRF *vs* SR-XRF.

Variations in sulphur

Trace elements in stalagmites can be used as annual chronological markers by providing clear annual cycles [38][39], which is helpful for deriving high-resolution chronologies [40] to complement traditional $\delta^{13}C$ and $\delta^{18}O$ stable isotope proxies [41]. To investigate whether variations in sulphur at sub-annual scales was practical for benchtop micro-XRF, sulphur concentrations were compared with those measured using SR-XRF in the period equivalent to 1800 to 1820. Annual patterns of sulphur

can be observed (**Figure 7A**) as the hydrology and ventilation regime have the same seasonality. An annual decrease of the sulphur concentration can be related to seasonal changes in drip water pH, or saturation state control on sulphur incorporation into calcite, due to an inferred competition between sulphate and bicarbonate at the calcite surface [42]. While the spatial resolution from the benchtop micro-XRF (**Figure 7B**) is inferior to that available from a synchrotron X-ray source (<5 microns), for speleothems with wide enough annual laminae, the features are generally consistent between both techniques, and correspond with the expected annual variation in the laminae.

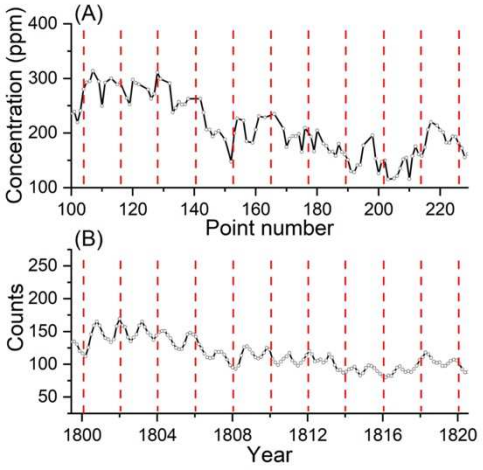

Figure 7. Sulphur variations of the reference stalagmite YD-S2 for the period 1800-1820 measured by (A) micro-XRF using 20 μm spot size, 10 μm step size; (B) SR-XRF with an estimated spot size of 7 μm. The red dash lines denote the start of each year.

XRF Mapping of Sulphur

Compared to linescans, mapping the distribution of sulphur over an entire stalagmite section has the advantage of identifying artefacts that fail to correspond to the laminae. A 22.6 x 10.1 mm mapping analysis on sulphur was carried out on polished QU_test1 using benchtop micro-XRF in the region shown in **Figure 1B**. Despite compromises in the measurement time to enable mapping to be completed in less than 24 hours, clear sulphur bands can be observed in the map corresponding to the laminae in the white light image of QU_test1 (**Figure 8A**), and a slight depletion of calcium can be observed in regions with higher sulphur concentration (**Figure 8B**).

In addition to the growth laminae, the map produced numerous random bright regions suggestive of high sulphur concentration. The intense sulphur spots in the micro-XRF map correspond to low calcium values suggesting that some variation in the calcite matrix may be a factor. Variations may include porosity, sample topography [44] and variation in crystallite orientation leading to diffraction artefacts [30][45]. When measuring stalagmites using benchtop micro-XRF, elemental composition,

matrix crystallinity and porosity can all have an impact on the X-ray fluorescence measured from the sample.

To investigate whether the random bright spots reflect rich sulphur deposition, or are artifact signals, sulphur mapping analysis was repeated using the second detector on the instrument. Each of the two detectors are placed in a specific angle to ensure incident X-Ray angle and the fluorescent X-ray angle is 90° [46]. As a result, each detector collects the fluorescing X-rays at a different angle, relative to the sample. If the sample comprises highly-oriented calcite crystallites, these would diffract the incident X-ray in a specific direction producing diffraction peaks that overlap with the sulphur K line. This directionaility can be tested by changing the angle of detection, using detector two on the instrument. This is indeed the case, as shown by comparing the XRF map from detector two where most of the bright regions are removed (**Figure 8C**) compared to the previous map from detector one (**Figure 8A**). It clear that the angle of detection can have a significant impact on the quality of the maps if the purpose of a study is to identify the laminae on a stalagmite. The same test for diffraction could be readily accomplished on an instrument with a single detector by measuring the sample in two orientations on the stage.

The mineral form of sulphur in the calcite matrix was investigated using XRD and Raman experiments. An XRD measurement of the polished sample surface of QU_test1 showed traces of magnetite in a calcite matrix with no aragonite. However, the sulphur minerals were below detection (Supporting Data, **Figure S1A**) as sensitivity of XRD is around 1 wt%. Compared to the bulk surface measurement provided by XRD, Raman mapping techniques can provide higher sensitivity if phases are concentrated at specific regions on the surface. As expected, the main peak in the average Raman spectrum of the sample was that of calcite at 1080 cm^{-1} (Supporting Data, Figure **S2A-B**). However, two weak, overlapped peaks were also observed at lower energy: a stronger peak at 1018 cm^{-1} corresponding to anhydrite ($CaSO_4$) and a shoulder at 1009 cm^{-1} diagnostic for gypsum ($CaSO_4.2H_2O$) [43]. Mapping the intensity of the anhydrite peak at 1018 cm^{-1} produces the same laminae structure to as that seen in the sulphur micro-XRF mapping (**Figure 8D**). This correlation between techniques supports the assignment of anhydrite , with a lesser quantity of gypsum, as the mineral source of sulphur in the laminae revealed by micro-XRF. The association with anhydrite also suggests that sulphur forms an alteration thin layer on the top of the stalagmite calcite matrix, which can explain the observed negative association of S and Ca (**Figure 8B-C**) as Ca is less abundant in anhydrite than calcite and Ca X-rays are more absorbed within anhydrite than the calcite matrix.[47]

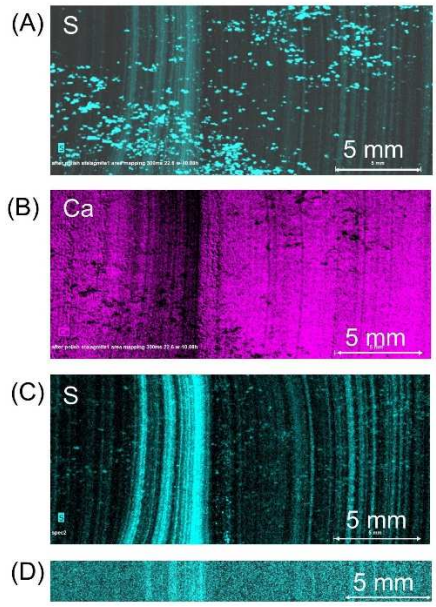

Figure 8. Micro-XRF mapping of polished QU_test1. Micro-XRF mapping of sulphur (A) and calcium (B) using detector one; Micro-XRF mapping of sulphur using detector two (C); (E) Raman map of the 1018 cm^{-1} peak intensity.

Two-dimensional mapping has clear advantages over a linescan when identifying features arising from cracks, pores or highly orientated crystallites that are unrelated to the laminae on the stalagmite surface. In order to improve the quality of the laminae features in these images, a multiple point statistics (MPS) approach [48] was used to gap-fill the scatter and produce a cleaner sulphur map. The unwanted artefacts (yellow zones in **Figure 9A**) were detected with a constant threshold filter and a morphological dilation operation, which grows the zones selected with the threshold by adding a 3-5 pixel layer to their borders. Note that this filter combination needs to be manually set up and possibly modified to select efficiently the zones recognized as artifacts, which can vary from image to image and can be similar to naturally occurring high/low-concentration zones. Data in the detected zones are then removed and replaced by stochastically simulated values. This was achieved by randomly sampling data from the "clean" parts of the image showing similar spatial structures as those surrounding the missing data. The sampled data are then assigned to the gaps to recover the missing textures (**Figure 9B**).

Although this was a supervised, rather than fully automated process, the MPS approach successfully removed the porosity artefacts to produce an acceptable image of sulphur distribution in laminae. This novel use of MPS may also prove useful in future for improving SR-XRF maps for laminae analysis. However, given the significant changes made to the image, and the somewhat subjective nature of the supervision, the authors would always recommend that the unmodified image be published alongside the MPS image as in **Figure 9**.

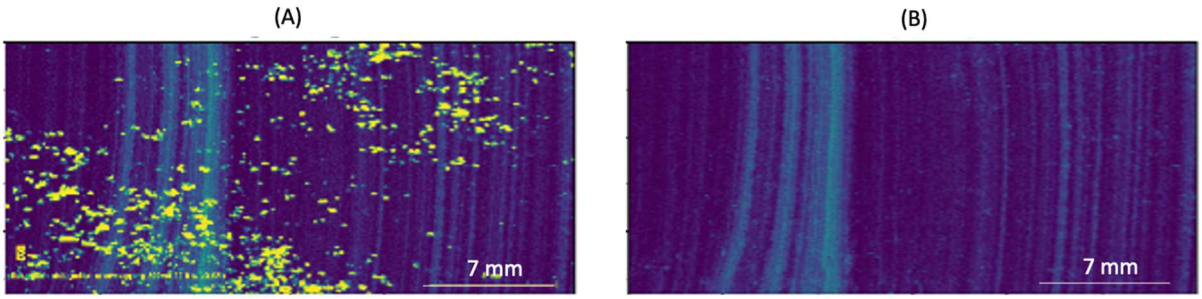

Figure 9. Sulphur mapping for stalagmite QU_test1 (A) before and (B) after MPS gap filling.

Conclusion

Benchtop micro-XRF was thoroughly investigated as a tool to examine variation of sulphur at trace levels along a stalagmite growth axis. Instrument parameters, including X-ray tube voltage and current were optimised to solve the challenge of trace sulphur detection in a calcite-rich sample matrix. Calibration was carried out using synthetic matrix matched standards to improve the accuracy of trace sulphur quantification analysis with detection limit as low as 73 ppm. The effect of roughness on the sample surface produced sulphur concentration spikes that were largely removed after polishing. A point-by-point transect analysis by benchtop micro-XRF showed good correlation with an equivalent SR-XRF transect of the same sample. Capturing seasonal variations in sub-annual data suggests that sulphur analysis by micro-XRF might be an efficient tool to develop chronologies from suitable stalagmites, especially fast-growing stalagmites with narrow laminae likely to be found at low latitudes.

A second stalagmite was used to investigate the use of micro-XRF mapping of sulphur. An XRD measurement was unable to confirm the mineral origin of the sulphur in this sample, however, Raman mapping of anhydrite and gysum correlated with the micro-XRF maps of sulphur. In addition to the sulphur laminae, micro-XRF mapping revealed regions of high sulphur concentration, even on a polished sample. Use of the second detector placed at a different angle relative to the sample demonstrated that the artefacts were mainly due to preferred orientation of crystallites diffracting the incident beam and interfering with the sulphur K line in the XRF spectrum. A multiple point statistics approach successfully filtered out artifacts unrelated to the laminae. This research demonstrates the potential of micro-XRF as an accessible option for analysis of sulphur in stalagmites for reconstruction of past climate and environmental changes, and an effective screening tool for SR-XRF.

Acknowledgments

The authors thank Sirine Fakra, Andrea Borsato and Katie Coleborn for their assistance with the mapping performed on beamline 10.3.2 at the Advanced Light Source, Lawrence Berkeley National

Laboratory in California, USA. Sirine Fakra processed the synchrotron scans. This work was partially funded through the Australian Research Council Discovery Project DP200100203. Access to the Advanced Light Source synchrotron was under experiment ALS-10166 with travel funding provided by the International Synchrotron Access Program (ISAP) managed by the Australian Synchrotron, part of ANSTO, and funded by the Australian Government. This research used resources of the Advanced Light Source, a U.S. DOE Office of Science User Facility under contract no. DE-AC02-05CH11231.

References

[1] I.J. Fairchild, P.C. Treble, Trace elements in speleothems as recorders of environmental change, Quaternary Sci. Rev., 28 (5-6) (2009), 449-468, https://doi.org/10.1016/j.quascirev.2008.11.007.

[2] A. Baker, G. Mariethoz, L. Comas-Bru, A. Hartmann, S. Frisia, A. Borsato, P.C. Treble, A. Asrat, The Properties of Annually Laminated Stalagmites-A Global Synthesis. Rev. Geophys., 59 (2) (2021) p.e2020RG000722, https://doi.org/10.1029/2020RG000722.

[3] S. Frisia, A. Borsato, I.J. Fairchild, J.J.E. Susini, P.S. Letters, Variations in atmospheric sulphate recorded in stalagmites by synchrotron micro-XRF and XANES analyses. 235 (3-4) (2005) 729-740, https://doi.org/10.1016/j.epsl.2005.03.026.

[4] S. Frisia, A. Meibom, Atmospheric sulphate increase in the past 200 years recorded in stalagmites from Italy and Oman; European Geosciences Union, General Assembly, Vienna, Austria, April 2-7 (2006).

[5] I.J. Fairchild, C.L. Smith, A. Baker, A. L. Fuller, C. Spötl, D. Mattey, F. McDermott, Modification and preservation of environmental signals in speleothems, Earth-Sci Rev., 75 (1-4) (2006) 105-153, https://doi.org/10.1016/j.earscirev.2005.08.003.

[6] A. Borsato, S. Frisia, P.M. Wynn, I.J. Fairchild, R. Miorandi, R., Sulphate concentration in cave dripwater and speleothems: long-term trends and overview of its significance as proxy for environmental processes and climate changes. Quaternary Sci. Rev., 127 (2015) 48-60, https://doi.org/10.1016/j.quascirev.2015.05.016.

[7] P.M. Wynn, A. Borsato, A. Baker, S. Frisia, R. Miorandi, I.J. Fairchild, Biogeochemical cycling of sulphur in karst and transfer into speleothem archives at Grotta di Ernesto, Italy. Biogeochemistry, 114 (1-3) (2013) 255-267, https://doi.org/10.1007/s10533-012-9807-z.

[8] P.M. Wynn, I.J. Fairchild, S. Frisia, C. Spötl, A. Baker, A. Borsato, J. C. G., High-resolution sulphur isotope analysis of speleothem carbonate by secondary ionisation mass spectrometry, Chem. Geol., 271 (3-4) (2010), 101-107, https://doi.org/10.1016/j.chemgeo.2010.01.001.

[9] P.C. Treble, I.J. Fairchild, A. Baker, K.T. Meredith, M.S. Andersen, S.U Salmon, C. Bradley, P.M. Wynn, S.I. Hankin, A. Wood, E. McGuire, Roles of forest bioproductivity, transpiration and fire in a nine-year record of cave dripwater chemistry from southwest Australia, Geochim. Cosmochim. Acta, 184 (2016) 132-150, https://doi.org/10.1016/j.gca.2016.04.017.

[10] M.S. Roberts, P.L. Smart, A. Baker, Annual trace element variations in a Holocene speleothem, Earth Planet. Sc. Lett., 154 (1-4) (1998) 237-246, https://doi.org/10.1016/S0012-821X(97)00116-7.

[11] F. Ban, A. Baker, C.E. Marjo, W. Duan, X. Li, J. Han, K. Coleborn, R. Akter, M. Tan, G. Nagra, An optimized chronology for a stalagmite using seasonal trace element cycles from Shihua Cave, Beijing, North China. Sci. Rep., 8 (1) (2018) 1-9, https://doi.org/10.1038/s41598-018-22839-z.

[12] K.P. Jochum, D. Scholz, B. Stoll, U. Weis, S.A. Wilson, Q. Yang, A. Schwalb, N. Börner, D.E. Jacob, M.O. Andreae, Accurate trace element analysis of speleothems and biogenic calcium carbonates by LA-ICP-MS, Chem. Geol., 318 (2012) 31-44, https://doi.org/10.1016/j.chemgeo.2012.05.009.

[13] C.A. Craig, K.E. Jarvis, L.J. Clarke, An assessment of calibration strategies for the quantitative and semi-quantitative analysis of calcium carbonate matrices by laser ablation-inductively coupled plasma-mass spectrometry (LA-ICP-MS). J. Anal. At. Spectrom., 15 (8) (2000) 1001-1008, https://doi.org/10.1039/B002097O.

[14] A. Marín-Roldán, J.A. Cruz, J. Martín-Chivelet, M.J. Turrero, A.I. Ortega, J.O. Cáceres, Evaluation of Laser Induced Breakdown Spectroscopy (LIBS) for detection of trace element variation through stalagmites: potential for paleoclimate series reconstruction, J. Appl. Laser Spectrosc., 1 (2014) 7-12, http://hdl.handle.net/10261/113885.

[15] S. Qiao, Y. Ding, D. Tian, L. Yao, G. Yang, A review of laser-induced breakdown spectroscopy for analysis of geological materials, Appl. Spectrosc. Rev., 50 (1) (2015) 1-26, https://doi.org/10.1080/05704928.2014.911746.

[16] J.A. Cruz, J. Martín-Chivelet, A. Marín-Roldán, M.J. Turrero, R.L. Edwards, A.I. Ortega, J.O. Cáceres, Trace elements in speleothems as indicators of past climate and Karst hydrochemistry: a case study from Kaite Cave (N Spain). In Hydrogeological and environmental investigations in Karst systems (2015) pp. 569-577. Springer, Berlin, Heidelberg, https://doi.org/10.1007/978-3-642-17435-3_64.

[17] M. Greaves, S. Barker, C. Daunt, H. Elderfield, Accuracy, standardization, and interlaboratory calibration standards for foraminiferal Mg/Ca thermometry. Geochem. Geophys., 6 (2) (2005) 1-9, https://doi.org/10.1029/2004GC000790.

[18] J. Yu, J. Day, M. Greaves, H.J.G. Elderfield, Geochem. Geophys., Determination of multiple element/calcium ratios in foraminiferal calcite by quadrupole ICP-MS. 2005, 6 (8) 1-9, https://doi.org/10.1029/2005GC000964.

[19] A. Borsato, S. Frisia, I.J. Fairchild, A. Somogyi, J. Susini, Trace element distribution in annual stalagmite laminae mapped by micro-meter-resolution X-ray fluorescence: implications for incorporation of environmentally significant species. Geochim. Cosmochim. Acta, 71 (6) (2007) 1494-1512, https://doi.org/10.1016/j.gca.2006.12.016.

[20] A. Kuczumow, D. Genty, P. Chevallier, J. Nowak, C.U. Ro, Annual resolution analysis of a SW-France stalagmite by X-ray synchrotron microprobe analysis. Spectrochim. Acta B, 58 (5) (2003) 851-865, https://doi.org/10.1016/S0584-8547(03)00022-3.

[21] S. Badertscher, A. Borsato, S. Frisia, H. Cheng, R.L. Edwards, O. Tüysüz, D. Fleitmann, Speleothems as sensitive recorders of volcanic eruptions–the Bronze Age Minoan eruption recorded in a stalagmite from Turkey. Earth Planet. Sc. Lett., 392 (2014) 58-66, https://doi.org/10.1016/j.epsl.2014.01.041.

[22] S. Frisia, A. Borsato, J. Susini. Synchrotron radiation applications to past volcanism archived in speleothems: an overview. J. Volcanol. Geotherm. Res., 177 (1) (2008) 96-100, https://doi.org/10.1016/j.jvolgeores.2007.11.010.

[23] T.O. Richter, S. Van der Gaast, B. Koster, A. Vaars, R. Gieles, H.C. de Stigter, H. De Haas, T.C. van Weering, The Avaatech XRF Core Scanner: technical description and applications to NE Atlantic sediments. Geol. Soc. Spec. Publ., 267 (1) (2006) 39-50, https://doi.org/10.1144/GSL.SP.2006.267.01.03.

[24] R. Ortega, G. Devès, R. Maire, Nuclear microprobe analysis of uranium-rich speleothems: Methodological aspects. Nucl. Instr. Meth. B, 210 (2003) 455-458, https://doi.org/10.1016/S0168-583X(03)01075-9.

[25] A. Guilherme, G. Buzanich, M.L. Carvalho, Focusing systems for the generation of X-ray micro beam: An overview, Spectrochim. Acta B, 77 (2012) 1-8, https://doi.org/10.1016/j.sab.2012.07.021.

[26] N.J. de Winter, M. Sinnesael, C. Makarona, S. Vansteenberge, P. Claeys, Trace element analyses of carbonates using portable and micro-X-ray fluorescence: performance and optimization of measurement parameters and strategies. J. Anal. At. Spec., 32 (6) (2017) 1211-1223, https://doi.org/10.1039/C6JA00361C.

[27] J. Buckles, H.D. Rowe, Development and optimization of microbeam X-ray fluorescence analysis of Sr in speleothems. Chem. Geol., 426 (2016) 28-32, https://doi.org/10.1016/j.chemgeo.2016.02.003.

[28] G. Dandurand, R. Maire, R. Ortega, G. Devès, B. Lans, L. Morel, A.S. Perroux, N. Vanara, L. Bruxelles, S. Jaillet, I. Billy, X-ray fluorescence microchemical analysis and autoradiography applied to cave deposits: speleothems, detrital rhythmites, ice and prehistoric paintings. Geomorphol. Relief, Process. Environ., 17 (4) (2011) 407-426, https://doi.org/10.4000/geomorphologie.9623.

[29] S. Vansteenberge, N.J. de Winter, M. Sinnesael, Z. Xueqin, S. Verheyden, P. Claeys, Benchtop μXRF as a tool for speleothem trace elemental analysis: Validation, limitations and application on an Eemian to early Weichselian (125–97 ka) stalagmite from Belgium. Palaeogeogr. Palaeoclimatol. Palaeoecol., 538 (2020) 109460, https://doi.org/10.1016/j.palaeo.2019.109460.

[30] S. Frisia, A. Borsato, I.J. Fairchild, F. McDermott, Calcite fabrics, growth mechanisms, and environments of formation in speleothems from the Italian Alps and southwestern Ireland. J. Sediment. Res., 70 (5) (2000) 1183-1196, https://doi.org/10.1306/022900701183.

603 [31] M. Lipar, J.A. Webb, Middle–late Pleistocene and Holocene chronostratigraphy and climate
604 history of the Tamala Limestone, Cooloongup and Safety Bay Sands, Nambung National Park,
605 southwestern Western Australia. Aust. J. Earth Sci., 61 (8) (2014) 1023-1039,
606 https://doi.org/10.1080/08120099.2014.966322.
607 [32] G. Nagra, P.C. Treble, M.S. Andersen, P. Bajo, J. Hellstrom, A. Baker, Dating stalagmites in
608 mediterranean climates using annual trace element cycles. Sci. Rep., 7 (1) (2017) 1-12,
609 https://doi.org/10.1038/s41598-017-00474-4.
610 [33] G. Nagra, P.C. Treble, M.S. Andersen, I.J. Fairchild, K. Coleborn, A. Baker, A post-wildfire
611 response in cave dripwater chemistry. Hydrol. Earth Syst. Sci., 20 (7) (2016) 2745-2758,
612 https://doi.org/10.5194/hess-20-2745-2016.
613 [34] L. McDonough, P.C. Treble, A. Baker, A. Borsato, S. Frisia, G. Nagra, K. Coleborn, M. Gagan,
614 S.S. Fakra, D. Paterson, Past fires and post-fire impacts reconstructed from a southwest Australian
615 stalagmite. Earth ArXiv (2021), https://doi.org/10.31223/X5JC86.
616 [35] W.C. Ferguson, Archaeological investigations at the Quininup Brook site complex, Western
617 Australia. Rec. West Aust. Mus., 8(4) (1981) 609-637.
618 [36] M. Gravey, G. Mariethoz, QuickSampling v1. 0: a robust and simplified pixel-based multiple-
619 point simulation approach. Geoscientific Model Development, (2020) 13 (6), 2611-2630,
620 https://doi.org/10.5194/gmd-13-2611-2020.
621 [37] Willis, J. P.; Turner, K.; Pritchard, G., XRF in the workplace: A guide to practical XRF
622 spectrometry. PANalytical Australia (2011).
623 [38] P.C. Treble, J. Chappell, J.M.G. Shelley, Complex speleothem growth processes revealed by
624 trace element mapping and scanning electron microscopy of annual layers. Geochim. Cosmochim.
625 Acta, 69 (20) (2005) 4855-4863, https://doi.org/10.1016/j.gca.2005.06.008.
626 [39] I.J. Fairchild, A. Baker, A. Borsato, S. Frisia, R.W. Hinton, F. McDermott, A.F. Tooth, Annual to
627 sub-annual resolution of multiple trace-element trends in speleothems. J. Geol. Soc., 158 (5) (2001)
628 831-841, https://doi.org/10.1144/jgs.158.5.831.
629 [40] I.J. Fairchild, S. Frisia, A. Borsato A.F. Tooth, Geochemical Sediments and Landscapes. D.J.
630 Nash (Ed.), S.J. Maclaren (Ed.), Blackwell UK (2007) 200,
631 https://doi.org/10.1002/9780470712917.ch1.
632 [41] L. Tan, C.C. Shen, Y. Cai, L. Lo, H. Cheng, Z. An, Trace-element variations in an annually
633 layered stalagmite as recorders of climatic changes and anthropogenic pollution in Central China,
634 Quat. Res., 81 (2) (2014) 181-188, https://doi.org/10.1016/j.yqres.2013.12.001.
635 [42] P.M. Wynn, I.J. Fairchild, A. Borsato, C. Spötl, A. Hartland, A. Baker, S. Frisia, J.U. Baldini,
636 Sulphate partitioning into calcite: Experimental verification of pH control and application to
637 seasonality in speleothems. Geochim. Cosmochim. Acta, 226 (2018) 69-83,
638 https://doi.org/10.1016/j.gca.2018.01.020.

[43] B. Lafuente, R.T. Downs, H. Yang, N. Stone, The power of databases: the RRUFF project. In Highlights in mineralogical crystallography, Walter de Gruyter GmbH: (2016) 1-29, https://doi.org/10.1515/9783110417104-003.

[44] S.J. Kelloway, C.R. Ward, C.E. Marjo, I.E. Wainwright, D.R. Cohen, Calibration for ED-XRF profiling of coal cores for the Itrax Core Scanner, Powder Diffr., (2014) 29(S1), S28-S34, https://doi.org/10.1017/S088571561400089X.

[45] G.M. Hansford, Back-reflection energy-dispersive X-ray diffraction: a novel diffraction technique with almost complete insensitivity to sample morphology, J. Appl. Crystallogr., 44(3) (2011) 514-525, https://doi.org/10.1107/S0021889811012696.

[46] N.J. de Winter, P. Claeys. Micro X-ray fluorescence (μ XRF) line scanning on Cretaceous rudist bivalves: A new method for reproducible trace element profiles in bivalve calcite. Sedimentology 64.1 (2017) 231-251.

[47] R. A. Shivaramu, V. Ramprasath, Effective atomic numbers and mass attenuation coefficients of some thermoluminescent dosimetric compounds for total photon interaction. Nucl. Sci. Eng. 132.1 (1999), 148-153.

[48] G. Mariethoz, J. Caers, Multiple-point geostatistics: stochastic modeling with training images. John Wiley & Sons, USA, (2014), https://doi.org/10.1016/j.cageo.2015.06.010 and https://wp.unil.ch/gaia/mps/qs/.

Mapping sulphur in stalagmites using benchtop micro-XRF

Sulphur may capture past climate events

Sample polishing

X-ray current and voltage tuning

Multipoint statistics